Inorganic Chemistry

Article

pubs.acs.org/IC

# Synthesis, Structure, and Superconductivity in the New-Structure-Type Compound: $SrPt_6P_2$

Bing Lv,*[,†] BenMaan I. Jawdat,[†] Zheng Wu,[†] Maurice Sorolla, II,[‡] Melissa Gooch,[†] Kui Zhao,[†] Liangzi Deng,[†] Yu-Yi Xue,[†] Bernd Lorenz,[†] Arnold M. Guloy,[‡] and Ching-Wu Chu[†,§]

[†]Texas Center for Superconductivity and Department of Physics, University of Houston, Houston, Texas 77204-5002, United States

[‡]Texas Center for Superconductivity and Department of Chemistry, University of Houston, Houston, Texas 77204-5003, United States

[§]Lawrence Berkeley National Laboratory, Berkeley, California 94720, United States

Supporting Information

**ABSTRACT:** A metal-rich ternary phosphide, $SrPt_6P_2$, with a unique structure type was synthesized at high temperatures. Its crystal structure was determined by single-crystal X-ray diffraction [cubic space group $Pa\bar{3}$; $Z = 4$; $a = 8.474(2)$ Å, and $V = 608.51(2)$ Å$^3$]. The structure features a unique three-dimensional anionic $(Pt_6P_2)^{2-}$ network of vertex-shared $Pt_6P$ trigonal prisms. The Sr atoms occupy a 12-coordinate (Pt) cage site and form a cubic close-packed (face-centered-cubic) arrangement, and the P atoms formally occupy tetrahedral interstices. The metallic compound becomes superconducting at 0.6 K, as evidenced by magnetic and resistivity measurements.

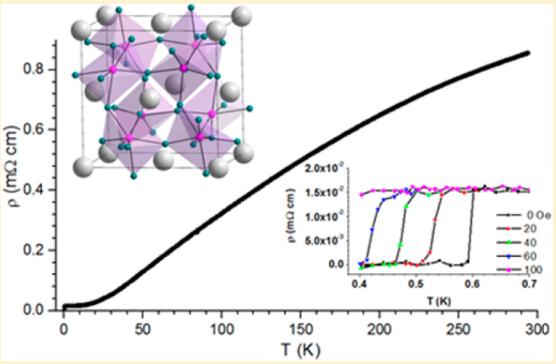


## 1. INTRODUCTION

Chemical systems that consist of an alkali metal (alkaline earth or rare earth), platinum, and a post-transition element X such as P, Ge, or B have yielded numerous new intermetallic and/or metal-rich compounds with a myriad of structural and bonding features. They include honeycomb lattices of $Pt_3X_3$ in EuPtP[1] and SrPtAs[2] ($AlB_2$-type), layers of tetrahedrally coordinated $Pt_4X_4$ in $SrPt_2Ge_2$[3] ($ThCr_2Si_2$-type) and $LaPt_2Ge_2$[4] ($CaBe_2Ge_2$-type), a three-dimensional anionic network of puckered hexagonal layers in CaPtGe[5] (TiNiSi-type), corner-shared ($XPt_5$) square pyramids in $DyPt_8P_2$,[6] a distorted perovskite ($XPt_6$) motif in noncentrosymmetric $Li_2Pt_3B$,[7] face-shared trigonal prisms ($XPt_6$) in $Li_4Pt_3Si$,[8] and propeller-shaped $Pt_7Si_3$ in $Ca_{10}Pt_7Si_3$.[9,10] The crystal symmetry and chemical coordination of these materials also vary with the valence of the cation. For instance, in the APtP compounds (A =Ca, Ba, La, Eu, and Lu),[1,11−13] the crystal symmetry changes dramatically from orthorhombic (space group $Pmc2_1$) for CaPtP[11] to cubic (space group $P2_13$) for BaPtP[11] and hexagonal (space group $P6_3/mmc$) for EuPtP[12,14] while the $PtP_3$ coordination is maintained. Therefore, an exploratory search in this class of materials may lead to the discovery of new compounds, which might enrich our chemical understanding of these Pt-related compounds.

On the other hand, novel physical properties have also been reported in various Pt-related compounds. For instance, a complex series of phase transitions appear in the mixed-valent EuPtP, i.e., three magnetic transitions[14] at 25, 8, and 0.9 K, following two first-order phase transitions[1] at 235 and 190 K, upon cooling, although these transitions have not yet been fully understood in detail. Superconductivity is observed in related Pt compounds such as SrPtAs,[2] $SrPt_2Ge_2$,[3] $CaPtSi_3$,[15] $SrPtGe_3$,[16] $Ca_2Pt_3Si_5$,[17] and $Li_2Pt_3B$[18] as well as in the strongly correlated electron systems $UPt_3$[19] and $CePt_3Si$.[20] The superconductivity in the noncentrosymmetric $CaPtSi_3$,[15] $SrPtGe_3$,[16] and $Li_2Pt_3B$[18] systems, particularly in the heavy Fermion $CePt_3Si$[20] compound, has generated great impact in the condensed matter physics field.

Herein we report the successful synthesis of a new ternary phase, $SrPt_6P_2$, which crystallizes in a new cubic structure [space group $Pa\bar{3}$ (No. 205)] displaying a unique three-dimensional network of vertex-shared $Pt_6P$ nominal trigonal prisms. This is an unprecedented Pt−P ternary compound that has corner-shared six-coordinated trigonal-prismatic coordination of $Pt_6P$,[21,22] and this contrasts the corner-shared octahedral (trigonal-antiprismatic) $Pt_6B$ coordination in $Li_2Pt_3B$[7] and face-shared trigonal-prismatic $Pt_6Si$ in $Li_4Pt_3Si$.[8] It is also different from the distorted antiperovskite $Pt_6P$ octahedral units in $SrPt_3P$.[23] Superconductivity at ~0.6 K, with low critical field, is observed for the title compound both magnetically and resistively.

**Special Issue:** To Honor the Memory of Prof. John D. Corbett

**Received:** October 1, 2014
**Published:** December 19, 2014

   dx.doi.org/10.1021/ic502377v | Inorg. Chem. 2015, 54, 1049−1054

## 2. EXPERIMENTAL METHODS

**Material Synthesis.** The title compound was initially discovered as a minor phase during our exploration attempt in the Sr−Pt−P ternary system when we work on the $SrPt_3P$ superconductors.[23] It was later synthesized phase pure by high-temperature reactions of stoichiometric Sr pieces (Alfa Aesar, 99.95%), Pt powder (Alfa Aesar, >99.95%), and prereacted $PtP_2$ from Pt and P powder (Sigma-Aldrich, >99.99%) within a clean $Al_2O_3$ crucible enclosed in a clean and dried fused-silica tube. A small piece of pure Zr foil (oxygen getter) was added at the opposite end of the fused-silica tube without contacting the reaction charge. Thereafter, the tube was sealed under vacuum. The tube was placed in a furnace, heated to 900 °C, kept at 900 °C for 4 days, then cooled at 20 °C/h to 400 °C, and finally quenched in ice water. To improve the homogeneity, the sample was reground, cold-pelletized, and then sintered following the previously described temperature profile. The resulting pellet is very dense (good for physical measurements) with an approximate density of ∼8.6 g/cm$^3$, ∼60% of its theoretical value. All synthesis procedures were carried out within a purified argon atmosphere glovebox with total $O_2$ and $H_2O$ levels of <0.1 ppm. Attempts to synthesis the isotypic $CaPt_6P_2$ and $BaPt_6P_2$ are unsuccessful, implying that the cation size might play an important role for stabilizing the structure.

**Single-Crystal X-ray Crystallography.** Powder X-ray diffraction (XRD) was performed using a Panalytical X'pert diffractometer. Single-crystal X-ray analysis was performed using a Siemens SMART diffractometer equipped with a CCD area detector. Monochromatic Mo K$\alpha_1$ radiation ($\lambda$ = 0.71073 Å) was used to collect a full hemisphere of data with the narrow-frame method. A single crystal of a typical size of 0.04 × 0.04 × 0.06 mm$^3$ was selected from the bulk samples, coated with paraffin oil to prevent deterioration in humid air, and mounted on a glass fiber using silicone glue. Data collection, cell refinements, and data reduction were performed using the Bruker *Apex2* software package. A hemisphere of 1271 frames was measured using a narrow-frame method with a scan width of 0.30° in $\omega$ and an exposure time of 60 s/frame. Final unit cell parameters were refined using 3327 reflections having $I > 10\sigma(I)$. The cubic cell parameters are $a$ = 8.474(2) Å, $V$ = 608.5(2) Å$^3$, $Z$ = 4, $\rho$ = 14.410 g/cm$^3$, and $2\theta_{max}$ = 56.88°.

The structure was solved by direct methods using *SHELXS97* with space group $Pa\bar{3}$ (No. 205) and refined using *SHELXS97* programs in the *WINGX* package. A $\psi$ scan was used for absorption correction. The structure solution was refined by full-matrix least-squares calculations on $F^2$, and the thermal motion of all atoms was treated anisotropically. The final $R$ indices converged to reasonable values [$I > 2\sigma(I)$], R1 = 0.0318 and wR2 = 0.0774, and $R$ indices [all data], R1 = 0.0343 and wR2 = 0.0786. The highest peak in the residual electron density map is located ∼0.8 Å away from the Pt atom and could not be assigned to any possible missing atom. All calculations were performed using the Siemens *SHELXTL* program package. The detailed crystal data and structure refinement for the title compound are listed in Table 1. Table 2 contains the atomic positions and equivalent displacement parameters for the title compound. The CIF and other detailed crystallographic information for the compound are provided in the Supporting Information (SI).

**Powder XRD.** Powder XRD data were collected using a Panalytical X'pert diffractometer (Cu K$\alpha$ radiation, flat-plate geometry) at room temperature equipped with an X'Celerator detector. Data were collected in the $2\theta$ range of 5−75°.

**Resistivity and Magnetic Measurements.** The electrical resistivity, $\rho$, as a function of the temperature, $\rho(T)$, and field, $\rho(H)$, was measured by employing a standard four-probe method from 300 K to 0.4 K under a magnetic field up to 7 T using a $He_3$ attachment in a Quantum Design Physical Property Measurement System. The alternating-current (ac) magnetic susceptibility at 15.9 Hz as a function of the temperature, $\chi(T)$, was measured by employing a compensated dual coil for mutual inductance measurement and using the Linear Research LR 400 bridge.

**Electronic Band-Structure Calculations.** Electronic band-structure calculations for $SrPt_6P_2$ were performed using the Stuttgart *TB-LMTO-ASA* program,[24] employing the tight-binding (TB) version of the linear muffin-tin orbital (LMTO) method in the atomic sphere approximation (ASA). The Barth−Hedin local exchange-correlation potential was implemented.[25] Radii of the atomic spheres and interstitial empty spheres were obtained as implemented in the *TB-LMTO-ASA* program. The tetrahedron method was selected for the $k$-space integration.[26] The calculations utilized basis sets Sr 5s/(5p)/4d/(4f), Pt 6s/6p/5d/(5f), and P 3s/3p/(3d) (downfolded orbitals in parentheses).[27] Reciprocal space integrations were performed using 249 irreducible $k$ points. The chemical bonding situations were investigated using the crystal orbital Hamilton population (COHP)[28] technique, as implemented in the *TB-LMTO-ASA 4.7* program package.[29]

**Table 1. Crystallographic Data for $SrPt_6P_2$**

| | |
|---|---|
| fw | 1320.10 |
| $T$, K | 293(2) |
| $\lambda$, Å | 0.71073 |
| cryst syst | cubic |
| space group | $Pa\bar{3}$ |
| $a$, Å | 8.474(2) |
| $\alpha$, deg | 90 |
| $V$, Å$^3$ | 608.5(2) |
| $Z$ | 4 |
| calcd density, g/cm$^3$ | 14.410 |
| abs coeff | 146.470 |
| $F$(000) | 2144 |
| index ranges | $-11 \le h \le 11$, $-11 \le k \le 11$, $-11 \le l \le 5$ |
| reflns colld/$R_{int}$ | 258/0.1070 |
| completion to $\theta$ = 25.25°, % | 100.0 |
| abs corrn | $\psi$ scan |
| max/min transmn | 0.9489/0.3308 |
| ref method | full-matrix least squares on $F^2$ |
| data/restraints/param | 258/0/16 |
| GOF | 1.223 |
| R1, wR2 for $I \ge 2\sigma(I)$ | 0.0318/0.0774 |
| R1, wR2 for all data | 0.0343/0.0786 |
| ext coeff | 0.00086(13) |
| largest diff peak/hole, e/Å$^3$ | 4.033/−2.428 |

**Table 2. Atomic Positions (×10$^4$) and Equivalent Displacement Parameters (Å$^2$ × 10$^3$) for $SrPt_6P_2$**

| atom | Wyckoff | $x$ | $y$ | $z$ | $U_{eq}$ |
|---|---|---|---|---|---|
| Pt | 24d | 3441(1) | 1571(1) | 790(1) | 4(1) |
| Sr | 4a | 0 | 0 | 0 | 6(1) |
| P | 8c | 8063(5) | 1937(5) | 6937(5) | 5(1) |

## 3. RESULTS AND DISCUSSION

Figure 1a shows the crystal structure of $SrPt_6P_2$. The arrangement of the Sr atom (4a site) corresponds to a face-centered-cubic (fcc) lattice. The P atoms (8c site) are located at nominal tetrahedral interstices, albeit displaced from the ideal tetrahedral site toward a triangular face. Pt atoms (24d site) form a unique network of P-centered, slightly distorted trigonal prisms linked through shared vertices (Figure 1b). The slightly distorted $Pt_6P$ unit exhibits an unusual atomic arrangement of two equilateral $Pt_3$ triangles with slightly different Pt−Pt distances [2.822(1) and 2.828(1) Å, respectively] lying above and below the P atom, with three longer Pt−P bonds [2.353(5) Å], three shorter Pt−P bonds [2.327(5) Å], and Pt−P−Pt bond angles of 73.7(2)° and 74.9(2)°, respectively. Furthermore, the two parallel $Pt_3$ equilateral triangles of the trigonal prism do not completely overlap when projected onto each


dx.doi.org/10.1021/ic502377v | *Inorg. Chem.* 2015, 54, 1049−1054

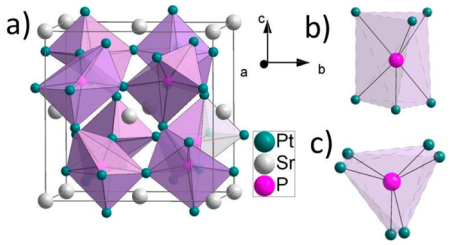


**Figure 1.** Crystal structure of $SrPt_6P_2$: (a) polyhedral ($Pt_6P$) representation of the unit cell; (b) side view of the $Pt_6P$ polyhedral building block; (c) top view of the $Pt_6P$ polyhedron.

other and are offset by 16.4° (Figure 1c); together, they form a distorted trigonal prism $Pt_6P$. The top-to-bottom Pt−P−Pt bond angles thus show slight deviations from the ideal bond angle 91.6° to 92.8(2)°. The Pt−P bonding distances are similar to the Pt−P distance in the previously reported $AlB_2$-type EuPtP[1] (2.358 Å) but shorter than the Pt−P distances in the TiNiSi-type LaPtP[11] (2.63−2.72 Å) and longer than those in $DyPt_8P_2$[6] (2.21−2.33 Å). The shortest Sr−P distance of 3.483(5) Å is slightly bigger, with Sr−P distances found in Sr/P Zintl phases in $Sr_3In_2P_4$[30] (3.03−3.25 Å) and SrIrP[31] (3.07−3.22 Å) . The Sr−Pt distances [3.2616(8) and 3.2742(8) Å] are comparable with those in related Sr/Pt ternary compounds.[2,3]

The building blocks in $SrPt_6P_2$ are reminiscent of the severely distorted $Pt_6X$ polyhedra[32] in the antiperovskite $Li_2Pt_3B$[7] and $SrPt_3P$[23] superconductors. In the $Li_2Pt_3B$ structure, the building blocks are severely distorted $Pt_6B$ octahedra; the equilateral $Pt_3$ triangles, which lie in parallel planes, are offset by 36.8° when projected onto each other, as opposed to the ideal $O_h$ of 60°. This observed angle is much larger than that observed in the title compound; on the other hand, in the related $Li_4Pt_3Si$ compound with the trigonal-prismatic $Pt_6Si$ as the building motif,[8] the $Pt_6$ trigonal prisms are less distorted than those of the title compound, with opposite $Pt_3$ triangles only offset by 9.4° (ideal $D_{3h}$ of 0°) when projected onto each other.

The connectivity of the $Pt_6P$ trigonal prisms in the title compound is different from the $Pt_6B$ (in noncentrosymmetric and cubic $Li_2Pt_3B$[7]) and the $Pt_6Si$ (in trigonal $Li_4Pt_3Si$[8]) in that the $Pt_6P$ network is centrosymmetric and cubic, which is incompatible with ideal trigonal prismatic symmetry. In the title compound $SrPt_6P_2$, the distorted $Pt_6P$ trigonal prisms are linked by the Pt vertices [with a P−Pt−P angle of 136.3(2)°] and form a $Pt_3P$ ("$Pt_{6/2}P$") network along all directions. The corner-shared $Pt_6P$ polyhedra form an −8-membered $Pt_4P_4$ ring. (Figure 2a). Consequently, a complicated unique three-dimensional framework is constructed in which a total of 12

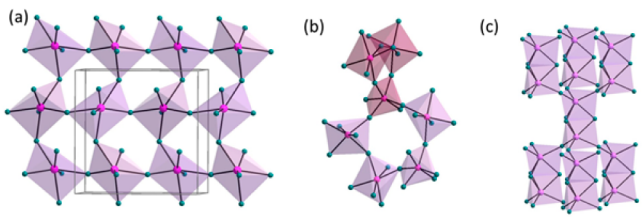


**Figure 2.** (a) $Pt_4P_4$ rings formed from corner-shared $Pt_6P$ polyhedra in $SrPt_6P_2$. (b) $Pt_5B_5$ and $Pt_3B_3$ rings formed from corner-shared $Pt_6B$ in $Li_2Pt_3B$ (the different $Pt_5B_5$ and $Pt_3B_3$ rings are indicated by different color shading). (c) Face- and corner-shared $Pt_6Si$ polyhedra in $Li_4Pt_3Si$.

corrugated $Pt_4P_4$ rings are formed around one central $Pt_6P$ building block, which is rather similar to the octahedral arrangement observed in the anti-$ReO_3$ structure.[33] On the other hand, the $Pt_6B$ octahedra in the $Li_2Pt_3B$[7] are also corner-shared through Pt vertices. These form a network with different $Pt_3B_3$ rings and $Pt_5B_5$ rings, with three planar $Pt_3B_3$ rings and nine corrugated $Pt_5B_5$ rings around each $Pt_6B$ octahedron (Figure 2b). In the $Li_4Pt_3Si$ structure,[8] the trigonal prisms $Pt_6Si$ are face-shared by the common $Pt_3$ triangle and form a $Pt_9Si_2$ ("$Pt_6Pt_3Si_2$") double unit, and the $Pt_9Si_2$ units are linked by the Pt vertices and form a different three-dimensional $Pt_3Si$ ("$Pt_{6/2}Pt_3Si_2$"= "$Pt_6Si_2$") network (Figure 2c).

The neighboring $Pt_4P_4$ rings form an irregular pseudocubic cage that is composed of a total of eight $Pt_6P$ polyhedra. The four $Pt_6P$ polyhedra on each of the six faces of the pseudocube are all bridged through Pt vertices and form the $Pt_4P_4$ ring. Therefore, a cavity site, which is equivalent to the A site of the perovskite structure, is created (Figure 3a). Similar to the

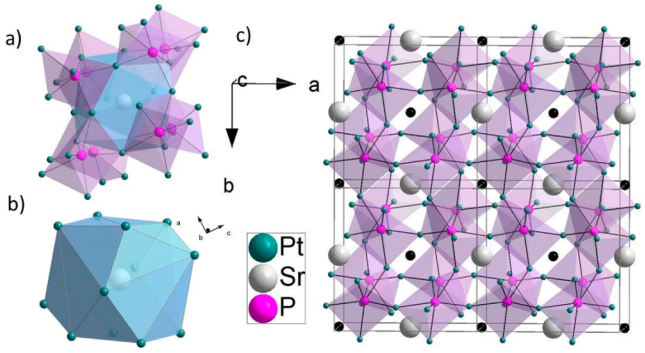


**Figure 3.** (a) Cavity sites (shaded blue) formed by the corner-shared $Pt_6P$ polyhedron. (b) Nearest-neighboring Pt atoms, which surround the Sr atoms, forming a distorted $Pt_{12}$ cuboctahedral polyhedron. (c) Extended lattice showing the Sr atoms alternately occupying half of the cavity sites. The other half of the cavity sites are highlighted by black spheres for illustration.

coordination number of the perovskite, the Sr atoms sit in the cavity sites with a total of 12 nearest-neighboring Pt atoms. The 12 Pt atoms constitute a highly distorted cuboctahedron with six Sr−Pt distances at 3.2616(8) Å and another six Sr−Pt distances at 3.2742(8) Å, as shown in Figure 3b. In the extended lattice, each $Pt_6P$ polyhedron is shared by eight neighboring $Pt_4P_4$ rings and has a formula of $\square(Pt_{6/2}P)_{8/8}$ = $\square(Pt_3P)$. The Sr atoms only occupy half of the cavity sites formed by $Pt_4P_4$ rings alternately and thus have a final formula of $Sr_{0.5}(Pt_3P)$ = $SrPt_6P_2$ (Figure 3c). It is interesting to note that there are only four crystallographic sites for the cubic space group $Pa\bar{3}$ (No. 205): 24d (occupied by Pt); 8c (occupied by P); 4a (occupied by Sr); 4b (another half-cavity site). The cavity site formed at the 4a site has a much larger Pt−Pt distance (~6.5 Å) across the distorted cuboctahedron than the Pt−Pt distance at the 4b cavity site (~3.98 Å). An arbitrary assignment of Sr atom occupation at the 4b site will result in much shorter Sr−Pt (~1.99 Å) and Sr−P (~2.84 Å) distances, which will destabilize the structure.

The closest structure type to $SrPt_6P_2$ is the well-known $Sr(NO_3)_2$ structure type[34] (isopointal relationship). The arrangement of Sr and P atoms in $SrPt_6P_2$ is identical with that of Sr and N atoms in $Sr(NO_3)_2$, corresponding to the fcc packing of Sr (4a site) and of P and N in tetrahedral interstices (8c site). The Pt atoms in $SrPt_6P_2$ and the O atoms in


dx.doi.org/10.1021/ic502377v | Inorg. Chem. 2015, 54, 1049−1054

$Sr(NO_3)_2$ also have the same site symmetries (24d site). However, the Pt positions differ from the O positions in that the O and N atoms are coplanar in the salt and the Pt atoms are not coplanar with, and are significantly displaced from, the P atoms in the metal. The noncoplanarity and accompanying displacement of the $Pt_3$ triangles from the P atom results in a network of trigonal prisms $[PPt_3]^-$ in $SrPt_6P_2$, in contrast to isolated trigonal-planar units of $[NO_3]^-$ in $Sr(NO_3)_2$[34] (or distorted trigonal-planar units in $SnSe_2O_6$[35]). Thus, the unique structure of $SrPt_6P_2$ can be regarded as a metal-rich phosphide structural (isopointal) analogue of a common oxide.

To understand the chemical bonding of the compound, electronic band-structure calculations were performed using the Stuttgart *TB-LMTO-ASA* program. The density of states (DOS) plots of $SrPt_6P_2$ with projected DOS (PDOS) of the Pt d and P s and p states are shown in Figure 4. The

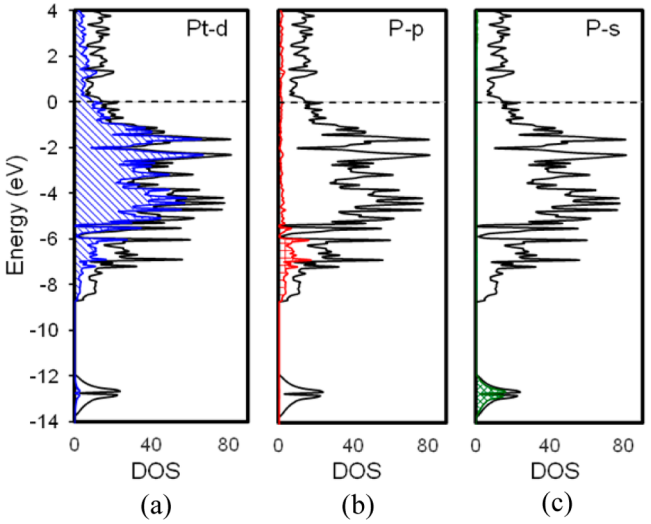


**Figure 4.** Calculated DOS and PDOS for $SrPt_6P_2$ using the LMTO method: (a) PDOS for Pt d states; (b) PDOS for P p states; (c) PDOS for P s states. Solid black line: total DOS. Shaded areas: PDOS. The Fermi level ($E_F$) is set at 0.0 eV.

calculations show that the compound is metallic, with the Fermi level near or just below a pseudogap. A simple formal electron-counting scheme of $Sr^{2+}$ and $P^{3-}$ ions results in a total formal electronic charge of $[Pt_6]^{4+}$ or $[Pt_3]^{2+}$ for every $Pt_3$ triangle. This is consistent with the calculated DOS and PDOS, which indicate that phosphorus-derived s and p states are essentially occupied with incompletely filled d bands of the Pt atoms. Studies on the chemical bonding of late-transition-metal polar intermetallics have shown that late transition metals like Pt usually exhibit negative oxidation states with filling of the d orbitals before the p states of the main-group metalloid.[36] In $SrPt_6P_2$, the p orbitals of P are sufficiently lower in energy and are completely filled. However, the incomplete filling or electron deficiency of the d states of Pt leads to interesting results.

Analysis of the chemical bonding in $SrPt_6P_2$ using the COHP method and its energy integral (ICOHP) clearly indicates that the P−Pt interatomic contacts within the $[Pt_6P]$ trigonal prisms are strongly bonding and essentially optimized interactions (Figure 5). However, the COHP plots of Pt−Pt interactions indicate significant bonding interactions within the planar triangles of the $Pt_6P$ trigonal prisms (ICOHP ∼ 0.74; Table 3). Moreover, the shortest Pt−Pt distance between neighboring

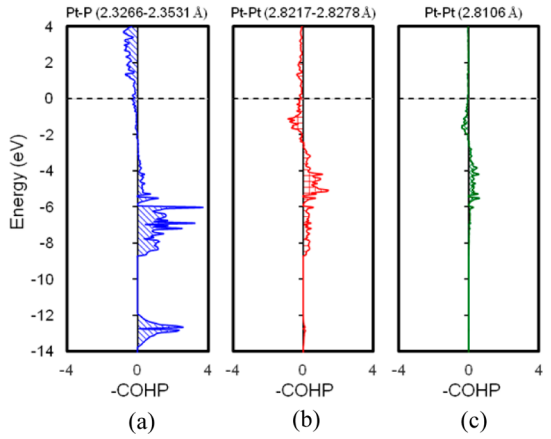


**Figure 5.** Calculated COHP curves for $SrPt_6P_2$: (a) COHP for P−Pt interactions; (b) COHP for Pt−Pt interactions within $Pt_3$ triangles; (c) COHP for Pt−Pt interactions between $Pt_3$ units of neighboring $Pt_6P$ trigonal prisms. Fermi level ($E_F$) is set at 0.0 eV.

**Table 3. Calculated ICOHP Values [eV/bond] of Relevant Interatomic Distances in $SrPt_6P_2$**

| atom pair | length (Å) | ICOHP |
|---|---|---|
| Pt−P (6×) | 2.327(5)−2.353(5) | 2.77 |
| Pt−Pt (3×) | 2.822(1)−2.828(1) | 0.74 |
| Pt−Pt (1×) | 2.811(2) | 0.49 |
| Pt−Pt (3×) | 3.388(1) | 0.03 |

$Pt_6P$ triangular prisms also shows significant bonding interactions (ICOHP ∼ 0.49). The structural nature of the bonding interaction between Pt−Pt atoms of neighboring triangles is shown in Figure 6. The close approach and bonds of

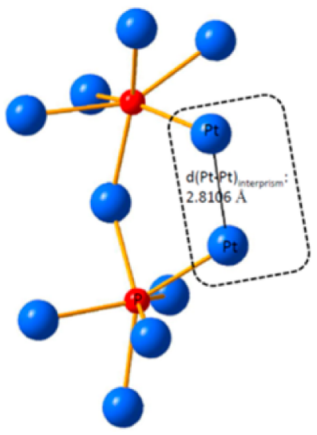


**Figure 6.** Pt−Pt bonding interactions between Pt atoms of neighboring $Pt_6P$ trigonal prisms. Color code: P, red; Pt, blue spheres.

the Pt atoms crowd into the 4e site and provide a rationale for the vacancy of the body-centered-cubic site. COHP analysis also shows that the Pt−Pt interactions between $Pt_3$ triangles of a $Pt_6P$ trigonal prism [Pt−Pt distance = 3.388(1) Å] are essentially nonbonding (ICOHP ∼ 0.03). Thus, the "electron deficiency" of the Pt atoms (unfilled d orbitals) is compensated for by the formation of Pt−Pt bonds within the triangular planes of the trigonal prisms and Pt−Pt atoms between neighboring trigonal prisms. The interprism Pt−Pt interactions coupled with the vacancy at the 4e site also provide an


dx.doi.org/10.1021/ic502377v | *Inorg. Chem.* 2015, 54, 1049−1054

electronic and geometric rationale for the observed distortions of the $Pt_6P$ trigonal prisms from ideality.

The as-synthesized powder shows a dark-gray color with a metallic luster and is stable in air. The diffraction peaks from the powder XRD pattern were well indexed without any noticeable impurity peaks and match well with the theoretical pattern generated from the structure of single-crystal XRD, as shown in Figure 7.

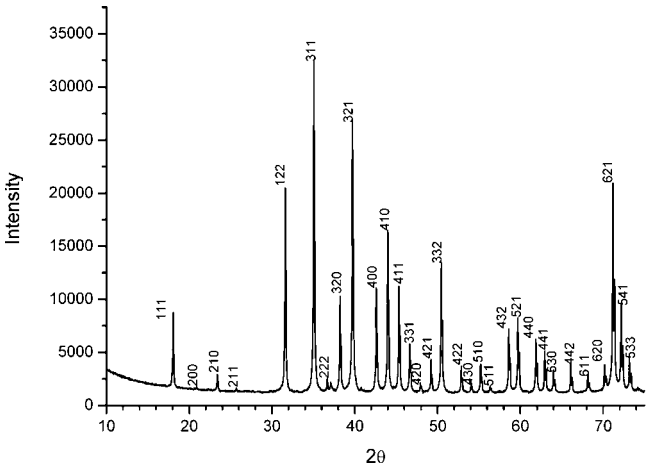


**Figure 7.** Powder XRD pattern with Miller indices for $SrPt_6P_2$.

The temperature-dependent resistivity, $\rho(T)$, of the title compound (Figure 8) at zero field, with a room temperature

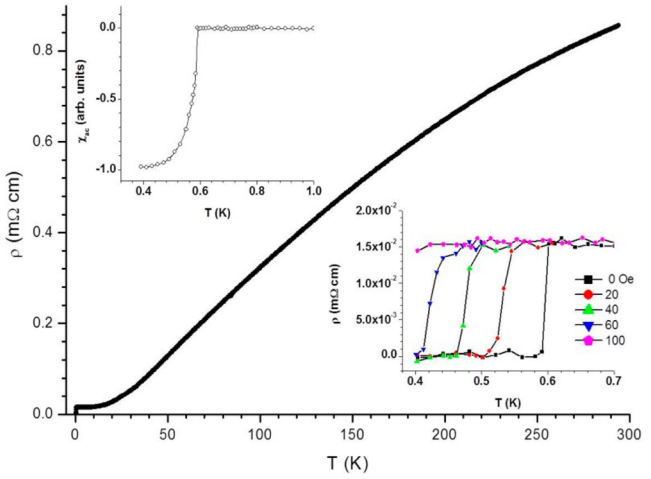


**Figure 8.** Resistivity $\rho(T)$ of $SrPt_6P_2$ from 0.4 to 290 K. Upper inset: ac susceptibility on a pelleted sample from mutual inductance measurements from 0.4 to 1.0 K. Lower inset: resistivity data under different magnetic fields between 0.4 and 0.7 K.

value of 0.85 mΩ·cm, decreases with temperature but with a strong negative curvature, suggesting possible strong electron correlation in the compound. The resistivity flattens between 8 and 0.6 K, and the residual resistivity is ~0.015 mΩ·cm. The relatively high value of the residual resistivity ratio, $\rho(290\ K)/\rho(5\ K) = 56$, suggests that the sample is of high quality. The resistivity drops sharply to zero below 0.60 K, with a transition width of less than 0.01 K at zero field, characteristic of a superconducting transition. In the presence of a magnetic field, the superconducting transition is systematically broadened, shifted to lower temperatures, and suppressed below 0.4 K at 100 Oe, as shown in the lower inset of Figure 8, suggesting a relatively low upper critical field of the title compound. In addition, the superconducting transition of $SrPt_6P_2$ was confirmed by the ac susceptibility measured through a mutual inductance technique down to 0.4 K, using the Linear Research LR 400 bridge. It displays a large and narrow diamagnetic shift at ~0.6 K with a tail nearly flat at 0.4 K, as shown in the upper inset of Figure 8, consistent with the $\rho(T)$ results and indicating the bulk superconducting nature of the materials. To the best of our knowledge, this is the first Pt-based pnictide superconductor with trigonal-prismatic building units.

## 4. CONCLUSIONS

In summary, a new ternary compound $SrPt_6P_2$ with a new structure type is synthesized through high-temperature solid-state reactions, and its crystal structure is determined by single-crystal XRD. The unique cubic crystal structure features an usual three-dimensional network of vertex-shared distorted $Pt_6P$ trigonal prisms analogous to the network of octahedral (antiprism) units in cubic perovskites. Furthermore, the title compound is isopointal, can be derived from the well-known $Sr(NO_3)_2$ structure type, and thus can be regarded as an intermetallic structural derivative of a common oxide. Superconductivity at 0.6 K is detected through both resistivity and magnetic susceptibility measurements. Given the unique crystallographic features of this perovskite-related structure type, further studies on compounds with related structures, and preferably with higher superconducting transition temperature, are in progress.

## ■ ASSOCIATED CONTENT

### Ⓢ Supporting Information

Crystallographic CIF file of $SrPt_6P_2$, details of the atomic coordinates and equivalent isotropic displacement parameters for $SrPt_6P_2$, anisotropic displacement parameters for $SrPt_6P_2$, and relevant bond lengths [Å] for $SrPt_6P_2$. This material is available free of charge via the Internet at http://pubs.acs.org.

## ■ AUTHOR INFORMATION

### Corresponding Author

*E-mail: blv@uh.edu.

### Notes

The authors declare no competing financial interest.

## ■ ACKNOWLEDGMENTS

The work in Houston is supported, in part, by U.S. Air Force Office of Scientific Research Grant FA9550-09-1-0656, the T. L. L. Temple Foundation, the John J. and Rebecca Moores Endowment, and the State of Texas through the Texas Center for Superconductivity at the University of Houston. B.L. also acknowledges the New Faculty Award by University of Houston. A.M.G. acknowledges the R. A. Welch Foundation (Grant E-1297).

## ■ REFERENCES

(1) Lossau, N.; Kierspel, H.; Langen, J.; Schlabitz, W.; Wohlleben, D.; Mewis, A.; Sauer, C. *Z. Phys. B: Condens. Matter* **1989**, *74*, 227−232.
(2) Ishikubo, Y. N.; Udo, K. K.; Ohara, M. N. *J. Phys. Soc. Jpn.* **2011**, *80*, 1−2.
(3) Ku, H. C.; Chen, I. a.; Huang, C. H.; Chen, C. W.; You, Y. B.; Tai, M. F.; Hsu, Y. Y. *Phys. C (Amsterdam, Neth.)* **2013**, *493*, 93−95.

(4) Imre, A.; Hellmann, A.; Mewis, A. *Z. Anorg. Allg. Chem.* **2006**, *632*, 2217−2221.
(5) Evers, J.; Oehlinger, G.; Polborn, K.; Sendlinger, B. *J. Alloys Compd.* **1992**, *182*, L23−L29.
(6) Imre, A.; Mewis, A. *Z. Anorg. Allg. Chem.* **2008**, *634*, 77−81.
(7) Eibenstein, U.; Jung, W. *J. Solid State Chem.* **1997**, *24*, 21−24.
(8) Dinges, T.; Hoffmann, R.-D.; Wüllen, L.; Henry, P.; Eckert, H.; Pöttgen, R. *J. Solid State Electrochem.* **2010**, *15*, 237−243.
(9) Doverbratt, I.; Ponou, S.; Lidin, S.; Fredrickson, D. C. *Inorg. Chem.* **2012**, *51*, 11980−11985.
(10) Fredrickson, D. C.; Doverbratt, I.; Ponou, S.; Lidin, S. *Crystals* **2013**, *3*, 504−516.
(11) Wenski, G.; Mewis, A. *Z. Anorg. Allg. Chem.* **1986**, *535*, 110−122.
(12) Imre, A.; Mewis, A. *Z. Naturforsch., B: J. Chem. Sci.* **2007**, *62*, 1153−1156.
(13) Wenski, G.; Mewis, A. *Z. Kristallogr.* **1986**, *176*, 125−134.
(14) Lossau, N.; Kierspel, H.; Michels, G.; Oster, F.; Schlabitz, W.; Wohlleben, D.; Sauer, C.; Mewis, A. *Z. Phys. B: Condens. Matter* **1989**, *77*, 393−397.
(15) Eguchi, G.; Peets, D. C.; Kriener, M.; Maeno, Y.; Nishibori, E.; Kumazawa, Y.; Banno, K.; Maki, S.; Sawa, H. *Phys. Rev. B* **2011**, *83*, 024512.
(16) Miliyanchuk, K.; Kneidinger, F.; Blaas-Schenner, C.; Reith, D.; Podloucky, R.; Rogl, P.; Khan, T.; Salamakha, L.; Hilscher, G.; Michor, H.; Bauer, E.; Hillier, A. D. *J. Phys.: Conf. Ser.* **2011**, *273*, 012078.
(17) Takeuchi, T.; Muranaka, H.; Settai, R.; Matsuda, T. D.; Yamamoto, E.; Haga, Y.; Onuki, Y. *J. Phys. Soc. Jpn.* **2009**, *78*, 085001.
(18) Lee, K.-W.; Pickett, W. *Phys. Rev. B* **2005**, *72*, 174505.
(19) Stewart, G. B.; Los, A. *Phys. Rev. Lett.* **1984**, *52*, 679−681.
(20) Bauer, E.; Hilscher, G.; Michor, H.; Paul, C.; Scheidt, E. W.; Gribanov, A.; Seropegin, Y.; Noel, H.; Sigrist, M.; Rogl, P. *Phys. Rev. Lett.* **2004**, *92*, 027003.
(21) Budnyk, S.; Prots, Y.; Kuz'ma, Y.; Grin, Y. *Z. Naturforsch., B: Chem. Sci.* **2002**, *57*, 1409−1413.
(22) Kuz'ma, Yu.; Chykhrij, S. Phosphides. In *Handbook on the Physics and Chemistry of Rare Earths*; Elsevier: Amsterdam, The Netherlands. 1996; Vol. *23*, pp 285−434.
(23) Takayama, T.; Kuwano, K.; Hirai, D.; Katsura, Y.; Yamamoto, A.; Takagi, H. *Phys. Rev. Lett.* **2012**, *108*, 237001.
(24) Jepsen, O.; Burkhardt, A.; Andersen, O. K. *The Stuttgart TB-LMTO-ASA Program*, version 4.7; Max-Planck-Institut für Festkörperforschung: Stuttgart, Germany, 1998.
(25) Barth, U. v.; Hedin, L. *J. Phys. C: Solid State Phys.* **1972**, *5*, 1629.
(26) Blöchel, P. E.; Jepsen, O.; Andersen, O. K. *Phys. Rev. B* **1994**, *49*, 16223.
(27) (a) Lambrecht, W. R. L.; Andersen, O. K. *Phys. Rev. B* **1986**, *34*, 2439. (b) Löwdin, P. *J. Chem. Phys.* **1951**, *19*, 1396.
(28) Dronskowski, R.; Blöchl, P. *J. Phys. Chem.* **1993**, *97*, 8617.
(29) Krier, G.; Jepsen, O.; Burkhardt, A.; Andersen, O. K. *The TB LMTO-ASA Program*, version 4.7; Max Planck Institute for Solid-State Research: Stuttgart, Germany.
(30) Cordier, G.; Schaefer, H.; Stelter, M. *Z. Naturforsch., B* **1986**, *41B*, 1416−19.
(31) Loehken, A.; Reiss, G. J.; Johrendt, D.; Mewis, A. *Z. Anorg. Allg. Chem.* **2005**, *631*, 1144−1148.
(32) Alvarez, S.; Alemany, P.; Casanova, D.; Cirera, J.; Llunell, M.; Avnir, D. *Coord. Chem. Rev.* **2005**, *249*, 1693−1708.
(33) Wells, A. F. *Structural Inorganic Chemistry*, 5th ed.; Oxford University Press: Oxford, U.K., 1984.
(34) Vegard, L. *Z. Phys.* **1922**, *9*, 395−410.
(35) Steinhauser, G.; Luef, C.; Wildner, M.; Giester, G. *J. Alloys Compd.* **2006**, *419*, 45−49.
(36) (a) Whangbo, M.-H.; Lee, C.; Köhler, J. *Angew. Chem., Int. Ed.* **2006**, *45*, 7465. (b) Köhler, J.; Whangbo, M.-H. *Solid State Sci.* **2008**, *10*, 444. (c) Köhler, J.; Whangbo, M.-H. *Chem. Mater.* **2008**, *20*, 2751. (d) Whangbo, M.-H.; Lee, C.-H.; Köhler, J. *Eur. J. Inorg. Chem.* **2011**, *2011*, 3841−3847.